Proceedings of the 21st ICSMGE, Vienna, Austria, 14 – 19 June 2026. Pistrol, Adam & Schweiger (eds.)
Published by: ÖGG, Austrian Society for Geomechanics, Salzburg, Austria, ISBN 978-3-9503898-4-5
https://doi.org/10.53243/ICSMGE2026-160

An in-situ estimation of the grain size distribution of a Martian regolith

Nicolas Verdier, Rémi Lapeyre, Emilien Gaudin, Charles Yana
Centre national d'études spatiales (CNES), Toulouse, France

Pierre Delage
Lab. Navier-CERMES, Ecole nationale des ponts et chaussées, Institut Polytechnique de Paris, France.
pierre.delage@enpc.fr

Véronique Ansan, Eric Beucler
Nantes Université, France

Khaled Ali, Matt Golombek, Eloise Marteau, K. Hurst, B.W. Banerdt
Jet Propulsion Laboratory, NASA – CalTech, Pasadena, USA

Constantino Charalambous
Imperial College, London, UK

Aymeric Spiga
Laboratoire de Météorologie Dynamique, IPSL, Sorbonne Université, CNRS, Paris, France

Eddy Constant
RTech, Verniole, France

Philippe Lognonné
Université Paris-Cité, Institut de Physique du Globe de Paris, CNRS, Paris, France

ABSTRACT: Various investigations have been conducted on the Martian regolith on the landing site of the NASA InSight mission on Mars. The InSight mission (2018 – 2022) is a geophysical mission aimed at better understanding the structure of Mars by using a broad band seismometer that provided new information about the planet's seismicity. Some information has also been gained on the regolith properties thanks, among other things, to two colour cameras and to the scoop placed at the end of the Instrument Deployment Arm (IDA) of the lander. To improve the quality of the signal provided by the seismometer, it was decided to bury the tether connecting it to the lander by pouring on it a pile of regolith using the IDA scoop. Detailed investigation of the regolith quantities extracted from the ground and poured onto the pile evidenced that some regolith particles (40%) has been blown out by the Martian wind, that was simultaneously recorded by the lander weather station. Numerical calculations were carried out to model the combined effects of (vertical) gravity and (horizontal) wind drag force on the falling particles. Unsurprisingly, it was showed that the largest particles felt below the scoop, forming a pile covering the tether, whereas smaller particles felt further away, the smaller the particles, the larger the distance, with silty and dust particles smaller than 100 micrometres blown away. Hence, a partial in-situ estimation of the grain size distribution of a soil was obtained for first time in extra-terrestrial conditions.

KEYWORDS: Mars, regolith, grain size distribution, wind, dump, pile.

1 INTRODUCTION

The InSight mission is a geophysical mission conducted by NASA with the support of the French and German Space Agencies (CNES and DLR, respectively), aimed at better understanding the structure of Mars (Banerdt et al. 2020). The InSight lander (see Figure 1) landed in a ~27-m-in-diameter, degraded impact crater in a Hesperian-Early Amazonian volcanic plain of the western Elysium Planitia (Golombek et al. 2020). Among other instruments, the InSight lander accommodated a very sensitive seismometer provided by CNES and IPGP (Paris Institute of Earth Physics), that was placed on the Mars ground by using the Instrument Deployment Arm (IDA). This seismometer recorded earthquakes and meteorite impacts during the mission (2018 – 2022). The other instrument seen on the ground is the so-called HP^3 device (Heat flow and Physical Properties Package) provided by DLR, consisting in a dynamic self-penetrating thermal probe aimed at measuring heat transfer at surface.

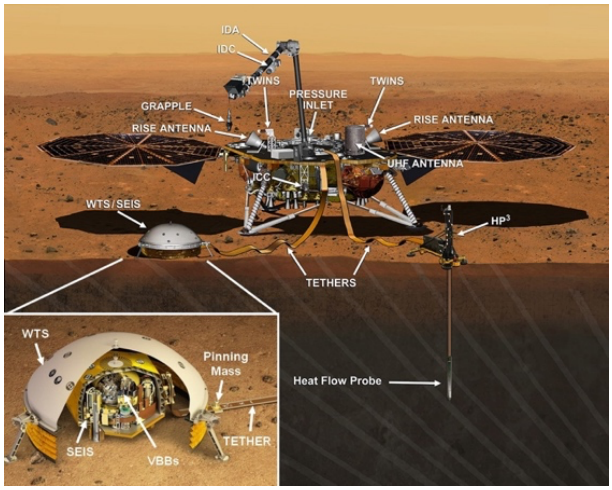

Figure 1. Artist view of the InSight lander with, among other devices, the two solar arrays, the detail of the seismometer SEIS under its Wind

and Thermal Shield (WTS), the IDA and the tethers connecting both the SEIS and the support system of the Heat Flow Probe (called HP^3), a self-penetrating dynamic penetrometer aimed at measuring the thermal properties at surface. Image credit NASA-JPL and IPGP D. Ducros (see Delage et al. 2024 for more details).

As described in Spohn et al. (2022), because of the lack of sufficient friction along the probe shaft, the penetration has only been possible, with the help of the IDA, along a little bit less than the 40 cm probe length.

Besides geophysical observations, significant information could also be gained on the mechanical properties of the surface regolith thanks to the lander cameras and by using the scoop placed at the end of the IDA (Delage et al. 2023, Golombek et al. 2023).

Interesting information was gained during an operation aimed at burying the tether connecting the seismometer to the lander (Yana et al. 2023) to reduce the perturbations due to the Martian wind (atmospheric pressure on Mars is 6 mb, with 95% CO_2) and to the large changes in temperature (around 100 °C) between night and day. Wind and temperature were continuously monitored by a weather station accommodated on the lander. Other important instrument used for geotechnical purposes are the two colour cameras, the Instrument Context Camera (ICC) placed on the lander, and the Instrument Deployment Camera (IDC), of better resolution, placed on the IDA (see Figure 1).

The detailed monitoring of the mass of regolith scraped from the surface and that poured on the tether evidenced some loss of grains due to the wind, which in turn allowed to better define the grain size distribution of the surface regolith of the InSight landing site.

2 THE REGOLITH AT THE INSIGHT LANDING SITE

The scheme of Figure 2 shows that planet regolith result from meteorite impacts on the ground, that progressively reduce the bedrock (basalt in the case of InSight) into a ground granular medium. For smaller impactors, the impact only affects the granular surface regolith with only granular ejecta around the crater, whereas larger impactors also impact the bedrock, resulting in having rocky ejecta around the crater.

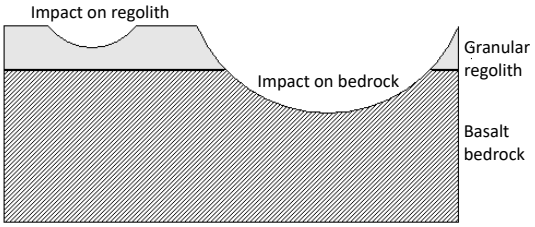

Figure 2. Scheme of the formation of planetary regolith.

The difference between craters can be observed in the photo of the fresh craters of Figure 4, with rocky ejecta around crater A (112 m diameter, with small black dots) and no rocky ejecta in crater B (75 m diameter). The depth at which ejecta is sourced in fresh craters is 0.084 times the diameter (Golombek et al. 2017), showing from crater B that the regolith thickness of larger than 6.3 m.

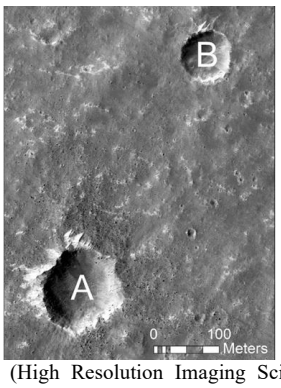

Figure 3. HiRISE (High Resolution Imaging Science Experiment) image showing a fresh crater (A, 112 m diameter) with rocky ejecta around and B (75 m, with no rocky ejecta around) (Golombek et al. 2017).

A typical profile illustrating the formation process presented in Figure 2 is shown in Figure 3, where one can see the basaltic bedrock (with a talus at its base), covered by a layer of blocky ejecta and, above, the granular regolith.

Further surface processes of the formation of regolith on Mars include weathering, erosion, grain saltation and sorting by gravity and winds (which is not the case on the Moon where there is no atmosphere).

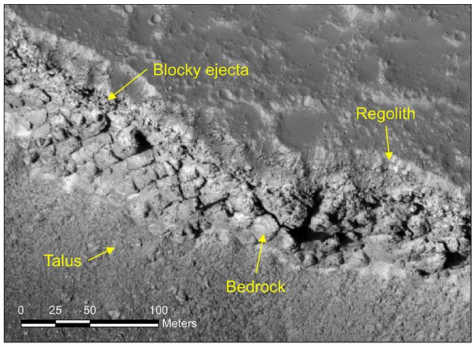

Figure 4. A portion of the exposed steep scarp in southern Utopia Planitia (Golombek et al. 2018).

Orbiter measurements of the thermal inertia I of the surface soils on Mars provided a first estimation of their grain size. Thermal inertia (unit $Jm^{-2}K^{-1}s^{-1/2}$) is given by:

$$I = \sqrt{k\rho c_p} \quad (1)$$

where k is the thermal conductivity, ρ the density, and c_p the specific heat capacity of the material. The principle that allows derivation of average particle size from thermal inertia is simple: for the same global mass, the changes in temperature of larger particles are slower than those of smaller ones. While density and specific heat capacity vary little, thermal conductivity can vary by orders of magnitude, depending on bulk porosity, composition, grain size (and also the state of cementation or induration).

Figure 5 shows a colour map of thermal inertia values characterised around the InSight landing site by the THEMIS (Thermal Emission Imaging System) instrument on board of the Mars Odyssey spacecraft launched in 2001 (e.g., Putzig & Mellon, 2007).

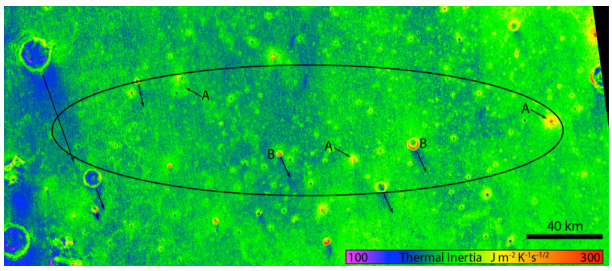

Figure 5. Thermal inertia map of the InSight landing area (Golombek et al. 2017) (the ellipse – 130 km in length and 27 km in width – is the zone where the lander may land, once the target on Mars has been fixed from the Earth).

One observes a green area of relatively constant thermal inertia with values between 160 and 230 J m^{-2} K^{-1} $s^{-1/2}$ (Golombek et al. 2017) that correspond to an average grain size of around 170 µm, showing that the surface is covered by a sandy regolith. In the Figure, high thermal inertia data are in red (*I* around 300 J m^{-2} K^{-1} $s^{-1/2}$). Some red dots can be observed in craters with rocky ejecta (A, B), comparable to the crater A in Figure 3.

The first direct observations of the soil on Mars were made through the cameras of the lander of the Viking 1 and 2 missions in 1976 (Moore and Jakoski 1989). More information was provided by subsequent missions from orbiters, landers or rovers. Most of the soils encountered are composed of dominantly sand size materials with some cohesion (Christensen & Moore, 2008). The sand is basaltic in composition, mostly 0.05 to 0.3 mm diameter (very fine to fine sand) and individual grains are generally equant to very equant and subrounded to rounded (e.g. Goetz et al., 2010; Ehlmann et al., 2017) confirming an origin via impact and aeolian activity (Golombek et al., 2020). Observation of most of the Martian aeolian bedforms (dunes, ripples, sand sheets...) showed that they are composed of 50 to 2 000 µm subrounded/rounded grains (e.g., Gough et al., 2021 in Gale crater, explored by Curiosity rover in 2012), with a preferential range of 50 – 350 µm for mobile active grains in ripples.

Figure 6 (Goetz et al. 2010) shows a photo obtained by the optical microscope of the Phoenix lander, showing that regolith particles have been rounded by long term wind saltation (a significant difference with Moon regolith that keep being quite angular in the absence of any atmosphere).

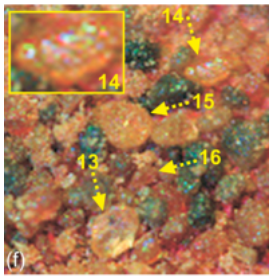

Figure 6. Microscopic observation of sub-rounded to rounded particles of Mars regolith at the Phoenix site. Picture width is 500 µm (Goetz et al. 2010).

3 TETHER BURIAL OPERATIONS

The tether burial operations are described in detail in Yana et al. (2023). Figure 7a shows a photo of the WTS taken on 14 March 2021, 816st day of the mission, i.e. at sol 816 – a sol is a Martian day, approximately equal to a terrestrial day – i.e. more than two years after landing. The photo has been taken by the Instrument Context Camera (ICC) located on the lander (see Figure 1), prior to the tether burial operations.

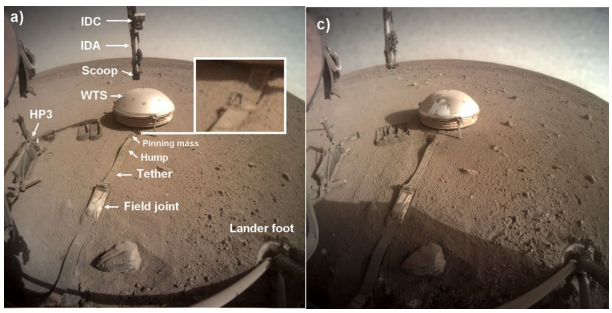

Figure 7. ICC images at two steps of the tether burial operations: (a) 14 March 2021, sol 816; (c) 16 May 2021 (Sol 877) after the sixth dump, with more scraps observed at the left of the WTS.

The photo shows that the landing area is flat with few rocks abundance at surface, as expected (Golombek et al. 2017). One of the lander feet can be seen on the bottom right, together with a rock that is not so far from the foot. One can see that the foot is embedded in the surface layer of granular regolith. The WTS is covered by dust (5 - 10 µm diameter) brought by wind (dust deposition was also quite critical on the solar arrays, leading to the end of the mission in December 2022 due to lack of energy production). One can also observe the tether connecting the seismometer to the lander (for energy providing and data transmission) and some scraps on the left of the WTS, made on the surface regolith by the scoop of the IDA.

Figure 7c taken on 16 May 2021 at sol 877 shows the tether covered after the six dumps that have been made on the tether, with more scraps observed on the left of the WTS. One can also observe that the WTS has been cleaned by some dumps made on it.

4 THE GRAIN SIZE DISTRIBUTION OF THE SURFACE REGOLITH

The determination of the grain size distribution (GSD) of the surface regolith during the tether burying operations was not initially planned. It has been an opportunistic investigation resulting from observing that the mass poured on the pit was smaller from that extracted from scraps. Given that a proportion of 40% of (finer) particles has been blown away by the wind, the GSD determined here only characterises larger particles, typically larger than 100 µm, as will be seen later on. A detailed analysis of the processes and calculations made to determine the GSD can be found in Verdier et al. (2023).

4.1 *Scraping*

The configuration of the scraps was defined in detail from the photos taken by the IDA camera by using Digital Elevation Models (DEMs), as seen in Figure 8.

The Figure shows both photos and DEMs prior scraping (a and d, respectively) and after scraping (b and e, respectively). The contour of the scoop extracted regolith is on red dash line. Figure 8f shows the difference between both DEMs, evidencing the shape of the mass of the extracted regolith. The volume contained in the scoop is not very well constrained due to the noise of the DEMs, the precision of their height (1 mm for each pixel) and the spatial delimitation of the extraction area whose width is estimated to be close to 2 mm. The average volume contained in the scoop is around 100 cm3, with a total volume reaching 652.5 ± 326.8 cm^3 for the six shovelings.

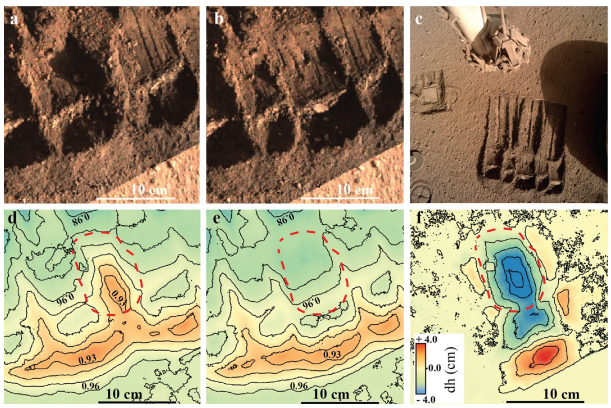

Figure 8. Quantification of the volume extracted by the scoop during dump 6. a) Photo before shoveling; b) Photo after shoveling; c) Global image of the scraps; d) DEM from image a); e) DEM from image b); f) DEM differencing between d) and e). The dashed red line contour indicates the scoop extracted regolith. Colours provide the depths in cm and the interval in contour lines is 1 cm.

4.2 *Shovelling and dumping*

To make sure that the tether is properly buried close to the WTS, the two first dumps were made on the WTS from a height of 55 cm, which resulted in cleaning it from dust, as seen in Figure 7c. The 4 following dumps were made from a height of 45 cm. The DEM of the pit after dump 6 is presented in Figure 9 (light comes from the right). The height of the pit is 4 cm with a basal surface of 334 cm^2 and the pit volume was estimated at 389.0 ± 234.3 cm^3.

When comparing it with that contained in the scoops during shovelling (i.e., 652.5 ± 326.8 cm^3), one observes that about 40% of the material is missing. This was related to the effect of the wind, measured and found equal to 5m/s.

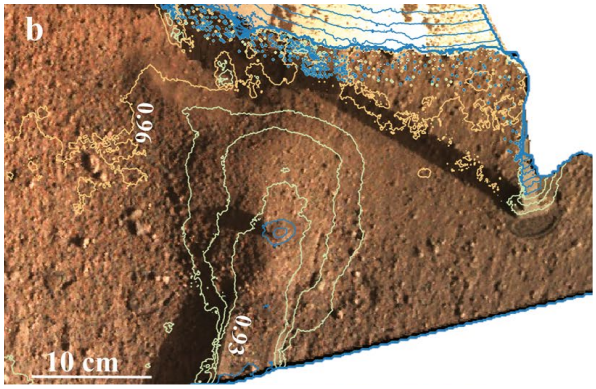

Figure 9. Image after dump 6, resulting in a final 4 cm high pile with a basal surface of 334 cm^2. Light comes from the right. Interval in contour lines is 1 cm.

The localisation of the plume made up of the fraction of regolith moved away by the wind from the pouring scoop and deposited was made possible by observing the wide-angle images provided by the ICC.

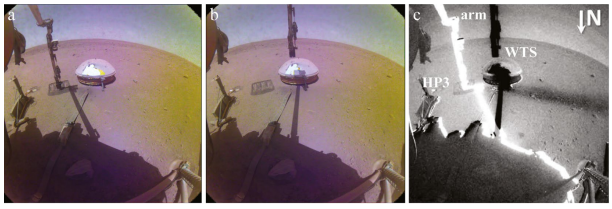

Figure 10. ICC images taken before (a) and after (B) dump 6. (c) image difference showing the dark plume made up of wind dispersed and transported particles.

Figure 10 illustrates such observations before (a) and after (b) dump #6. Although no significant change between both images could apparently be detected, their subtraction and magnification following a method developed by Charalambous et al. (2021) clearly evidences the changes that occurred. As seen in Figure 10c, the dispersed regolith appears like a dark plume, longer than the 1.25 m observed in the figure. The plume starts close to the deposited sand pile and is oriented along the wind direction provided by the lander sensor (coming from N140° - ESE to N320° - WNW). The widening shape of the plume along the wind direction is typical of aeolian plume deposits. The length of the plumes of transported and deposited particles observed from image analysis, is comprised between 1, 5 and 3 m, with wind speeds between 5 and 7 m/s.

4.3 *Determining the grain size distribution*

The principle of determining the grain size distribution is to use wind as a natural sorter thanks to drag effects. Particles mainly fall under the combined effects of gravity (g = 3.72 m/s^2 on Mars) and wind drag force, with the larger ones falling closer from the source and the smaller ones further on (interactions between particles and their effect on the wind are neglected for shake of simplicity). To do so, a model considering both actions has been developed for spherical particles in Verdier et al. (2023), in which all relevant equations are presented in detail.

Newton's law of motion for each grain is as follows:

$$M\vec{\gamma} = \rho_s V \frac{d\vec{v}}{dt} = \overrightarrow{F_w} + \vec{P} \quad (2)$$

where $\vec{\gamma}$ is the acceleration, ρ_s is the grain density (ρ_s= 3 Mg/m^3 for basalt), V the grain volume, $\vec{v}$ the grain velocity, $\overrightarrow{F_w}$ is the wind drag force and $\vec{P}$ the vertical downwards force due to gravity. $\vec{P}$ corresponds to the weight of the particle:

$$\vec{P} = \frac{\rho_s \pi D^3 g}{6}\vec{z} \quad (3)$$

where D is the particle diameter.

The horizontal wind drag force is proportional to the surface exposed to the wind (S = $\pi D^2/4$) and to the square of the horizontal wind velocity $w_s(z)^2$, through a drag coefficient C_d, as follows:

$$\overrightarrow{F_w} = \frac{\rho_{atm} C_d \pi D^2 w_s(z)^2}{6}\vec{z} \quad (4)$$

where ρ_{atm} is the atmosphere density, derived from the meteorological data from the weather station onboard the lander (Banfield et al. 2019).

The wind measurement is carried outat the height of the lander, i.e. 1.2 m above the ground, and a logarithmic correction is applied, according to Spiga et al. (2018):

$$w_s(z) = w_0 \frac{\ln\frac{z}{r}}{\ln\frac{z_s}{r}} \quad (5)$$

where z is the height of the ground, w_0 the wind speed measured at $z_s = 1.2\ m$ and r is the surface roughness, estimated equal to 1 cm (Charalambous et al. 2021).

The complete set of equations, presented in Verdier et al. (2023) has been solved by using the Simulink solver of Matlab. As an example, Figure 11 provides an output of calculations made with a wind of 5 m/s with 5500 grains, i.e. 500 grains for each of the size between 100 and 1000 µm indicated on the right side of the Figure. Unsurprisingly, the Figure shows that the largest grains (1 000 µm) fall directly below the scoop, whereas

smaller ones (100 µm) touch the ground at a distance between 4 and 4.5 m. This also shows that grains smaller than 100 µm (which indeed are in the range of aeolian loess particles) are blown away by the wind.

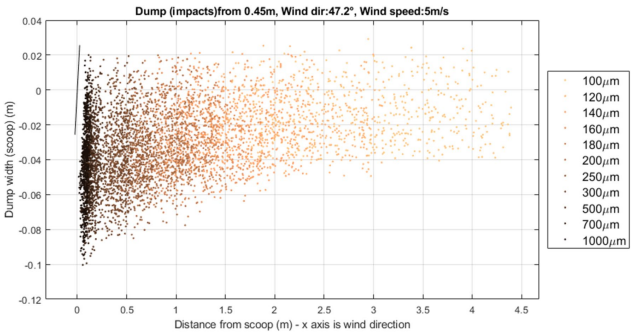

Figure 11. Simulation output of grain sorting by a 5m/s wind for 5 500 grains (500 grains for each 11 size mentioned in the legend). The colour of each grain depends on its size in the 100–1000 µm range. The *x* axis is in the mean wind direction.

The determination of the quantity of the particles sorted by the wind and deposited at a given distance from the scoop, based on the configuration of the plume (see Figure 10c) is more challenging. In a first approach, one can consider that the deposited particles are black and that the quantity of sorted particles at a given distance is proportional to the plume width. To improve this estimation, it was decided to decompose the plume into 4 grey levels. The areas corresponding to the two lower grey levels are considered without grains, that corresponding to the third grey level as a thin layer filled at 50% of dispersed regolith and the upper (black) zone like a full layer.

Figure 12 shows the relative ratios of particles sizes obtained for dump 6, with particles between 370 - 900 µm at 0.25 m from the scoop, and between 115 – 122 µm at 2.10 m.

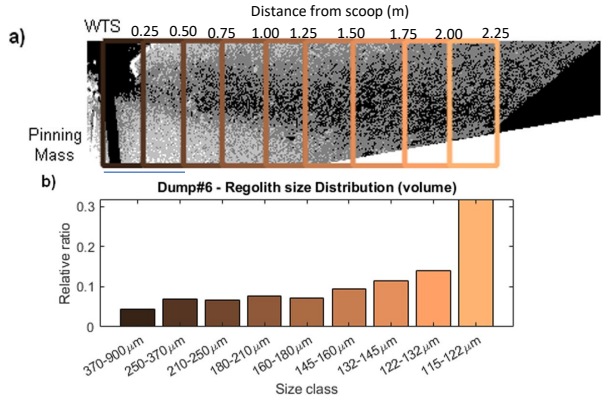

Figure 12. Grain size distribution from dump 6; a) Spatial distribution of grain size along the plume direction. Wind speed is 5.3 m/s. The colour of boxes is correlated to the grain size viewed in b; b) Volume frequency versus grain size.

The corresponding grain size distribution is given in Figure 13, together with those from dumps 3 and 4 (the identification of the plume of dump 5 was of poorer quality). As mentioned before, this GSD only characterises around 60% of the total particles, with those smaller than 100 µm blown away by the wind. The regolith exhibits a well sorted GSD with a significant proportion of particles around 120 – 140 µm, comparable on Earth to a fine sand like the Fontainebleau sand (France), that has been used as regolith simulant for InSight (Delage et al. (2017). Note also the good correspondence with the particles observed in Figure 6.

The Figure show some differences between the curves, that may due to local heterogeneities in the surface regolith extracted, but also to the uncertainties related to the image analysis of the plumes, from which the volumetric fraction were derived. The curves however shows that the main grain size is between 120 (dump 6) and 150 µm (dump 3), in reasonable agreement with preliminary estimation through the measurements of thermal inertia at surface (average diameter of 170 µm, see above).

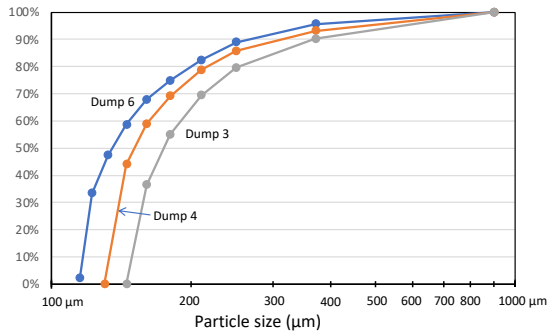

Figure 13. Cumulated grain size distribution curves from dumps 3, 4 and 6. The curves only characterises the ~60% fraction deposited on the ground. Particles smaller than 100 µm have been blown away.

5 CONCLUSIONS

Following previous contributions (e.g. Goetz et al. 2010, Weitz et al. 2018, Vaughan et al. 2023), this work provides further information on the grain size distribution of the Martian regolith at the InSight landing site. The operation of burying the tether connecting the seismometer of the InSight mission to the lander by using the scoop of the Instrument Deployment Arm of the lander provided an opportunity to indirectly work with grains separated during the pouring stage.

Since the volume of the piles poured by the different dumps did not fit with the mass extracted from the ground surface (with a loss estimated at 40%), it was concluded that some of the particles did not fall directly on the pile, but were blown and sorted by the wind (that was simultaneously measured in direction and speed by the lander weather station, and most often close to 5 m/s).

This sorting could be modelled by considering the movement of particles under the combined actions of gravity and wind drag force. The particle size was hence correlated to the distance from the scoop. This was however made under the simplistic hypothesis of free individual fall of spherical particles, neglecting the interactions between particles and their effect on the local air flow. In this regard, it seems that the modelled segregation is more severe than what really happens, and that the pile formed below the scoop was not only consisting in the largest particles (around 900 µm).

Another challenge was that of determining the volumes of the sorted particles deposited at a given distance. This was made based on the image analysis of the black plume formed along the wind direction. A strong hypothesis based on the grey levels measured was made, that can certainly be further elaborated through experimental simulations on the Earth.

Another limitation of the estimation is that we only characterised around 60% of the particles, with the 40% smaller than 100 µm blown away by the wind.

In spite of this uncertainties, the estimation provided by this approach, applied for three dumps, fitted reasonably well with pre-mission thermal inertia measurements.

6 ACKNOWLEDGEMENTS

This work was supported by the French space agency, Centre National d'Études Spatiales (CNES). Part of the research was carried out at the Jet Propulsion Laboratory, California Institute of Technology, under a contract with the National Aeronautics and Space Administration (80NM0018D0004).

7 REFERENCES

Banerdt, W. S., Smrekar, S., Banfield, D., Giardini, D., Golombek, M., Johnson, C. L., et al. (2020). Initial results from the InSight mission on Mars. *Nature Geoscience*, *23*(3), 183–189. https://doi.org/10.1038/s41561-020-0544-y

Banfield, D., Rodriguez-Manfredi, J. A., Rissel, C. T., Rowe, K. M., Leneman, D., Lai, H. R., et al. (2019). InSight auxiliary payload sensor suite (APSS). *Space Science Reviews*, *215*(4), 4. https://doi.org/10.1007/s11214-018-0570-x

Charalambous, C., McClean, J. B., Baker, M., Pike, W. T., Golombek, M., Lemmon, M., et al. (2021). Vortex-dominated Aeolian activity at InSight's landing site, Part 1: Multi-instrument observations, analysis, and implications. *Journal of Geophysical Research: Planets*, *126*(6). https://doi.org/10.1029/2020JE006757

Christensen, P.R., & Moore, H.J. (2008). The Martian surface layer. In H. H. Kieffer (Ed.), MARS (pp. 686-727). Tucson: University of Arizona Press.

Delage P., Karakostas F., Dhemaied A., Belmokhtar M., Lognonné P., Golombek M., et al. 2017. An investigation of the mechanical properties of some Martian regolith simulants with respect to the surface properties at the InSight mission landing site. *Space Science Reviews*, 211, 191-213, doi:10.1007/s11214-017-0339-7

Delage P. Caicedo B., Golombek M., Spohn T., Schmelzbach C., Brinkman N., Marteau E., Castillo-Betancourt J.-P., et al. (2023). Investigating the Martian soil at the InSight landing site. *Soils and Rocks*, https://doi.org/10.28927/SR.2024.005023 .

Ehlmann, B. L., Edgett, K. S., Sutter, B., Achilles, C. N., Litvak, M. L., Lapotre, M. G. A., et al. (2017). Chemistry, mineralogy, and grain properties at Namib and high dunes, Bagnold dune field, Gale crater, Mars: A synthesis of Curiosity rover observations. *Journal of Geophysical Research: Planets*, *122*(12), 2510–2543. https://doi.org/10.1002/2017JE005267

Goetz, W., Pike, W. T., Hviid, S. F., Madsen, M. B., Morris, R. V., Hecht, M. H., et al. (2010). Microscopy analysis of soils at the Phoenix landing site, Mars: Classification of soil particles and description of their optical and magnetic properties. *Journal of Geophysical Research: Planets,* 115(8), 1–23. https://doi.org/10.1029/2009JE003437

Golombek, M., Kipp, D., Warner, N., Daubar, I.J., Fergason, R., Kirk, R.L., Beyer, R., Huertas, A., Piqueux, S., Putzig et al. (2017). Selection of the InSight landing site. *Space Science Reviews*, 211(1-4), 5-95.http://dx.doi.org/10.1007/s11214-016-0321-9.

Golombek, M., Warner, N. H., Grant, J. A., Hauber, E., Ansan, V., Weitz, C. M., et al. (2020). Geology of the InSight landing site on Mars. *Nature Communications*, 11, 1–11. https://doi.org/10.1038/s41467-020-14679-1

Golombek, M., et al., 2023, Results from InSight robotic arm activities: Space Science Reviews, v. 219: 20, https://doi.org/10.1007/s11214-023-00964-0.

Gough, T. R., Hugenholtz, C. H., & Barchyn, T. E. (2021). Re-evaluation of large Martian ripples in Gale crater: Granulometric evidence for an impact mechanism and terrestrial analogues. *Journal of Geophysical Research: Planets*, *126* (12), e2021JE007011. https://doi. org/10.1029/2021JE007011

Moore, H. J., & Jakoski, B. M. (1989). Viking landing sites, remote-sensing observations, and physical properties of Martian surface materials. *Icarus*, *81*(1), 164–184. https://doi.org/10.1016/0019-1035(89)90132-2

Putzig, N.E., & Mellon, M.T. (2007). Apparent thermal inertia and the surface heterogeneity of Mars. *Icarus*, 191(1), 68–94, https://doi.org/10.1016/j.icarus.2007.05.013.

Spiga, A., Banfield, D., Teanby, N. A., Forget, F., Lucas, A., Kenda, B., et al. (2018). Atmospheric science with InSight. *Space Science Reviews*, *214*(109), 109. https://doi.org/10.1007/s11214-018-0543-0

Spohn, T., Hudson, T. L., Marteau, E., Golombek, M., Wippermann, T., Ali, K. S., et al. (2022). The HP^3 penetrator (Mole) on Mars: Soil properties derived from the penetration attempts and related activities. *Space Science Reviews,* 218(72), 72. https://doi.org/10.1007/s11214-022-00941-z

Vaughan, A., Minitti, M. E., Cardarelli, E. L., Johnson, J. R., Kah, L. C., Pilleri, P., et al. (2023). Regolith of the crater floor units, Jezero crater, Mars: Textures, composition, and implications for provenance. Journal of Geophysical Research: Planets, 128, e2022JE007437. https://doi.org/10.1029/2022JE007437.

Verdier N., V. Ansan, P. Delage, K.S. Ali, E. Beucler, C. Charalambouse al. (2023). Using wind dispersion effects during the InSight tether burial activities to better constrain the regolith grain size distribution. *Journal of Geophysical Research: Planets*, doi: 10.1029/2022JE007707

Weitz, C. M., Sullivan, R. J., Lapotre, M. G. A., Rowland, S. K., Grant, J. A., Baker, M., & Yingst, R. A. (2018). Sand grain sizes and shapes in Eolian Bedforms at Gale crater, Mars. Geophysical Research Letters, 45, 9471–9479. https://doi.org/10.1029/2018GL078972

Yana, C., Lapeyre, R., Gaudin, E., Hurst, K., Lognonné, P., & Rochas, L. (2023). Deployment and surface operations of the SEIS instrument onboard the InSight mission. *Acta Astronautica*, 202, 772–781. https://doi.org/10.1016/j.actaastro.2022.10.010